LETTER

Castration-mediated IL-8 Promotes Myeloid Infiltration and Prostate Cancer Progression

Keywords: androgen receptor, CXCL8, CXCR2, immunotherapy, PMN-MDSCs, myeloid-derived suppresor cells.

Zoila A. Lopez-Bujanda[1,2,3], Michael C. Haffner[1], Matthew G. Chaimowitz[3], Nivedita Chowdhury[1,2,3], Nicholas J. Venturini[3], Aleksandar Obradovic[3], Corey S. Hansen[4], Joanna Jacków[4], Karen S. Sfanos[1,5], Charles J. Bieberich[6,7], Paula J. Hurley[5], Mark J. Selby[8], Alan J. Korman[8,9], Angela M. Christiano[4,10], Angelo M. De Marzo[1,5], and Charles G. Drake[3,11,12].

[1]Department of Pathology, Johns Hopkins University School of Medicine, Baltimore, MD, USA; [2]Bloomberg-Kimmel Institute for Cancer Immunotherapy, Johns Hopkins University, Baltimore, MD, USA; [3]Columbia Center for Translational Immunology, Columbia University Medical Center, New York, NY, USA; [4]Department of Dermatology, Columbia University, New York, NY, USA; [5]Departments of Urology and Oncology, Johns Hopkins University School of Medicine, Baltimore, MD, USA; [6]Department of Biological Sciences, University of Maryland Baltimore County, Baltimore, Maryland; [7]University of Maryland Marlene and Stewart Greenebaum Cancer Center, Baltimore, Maryland; [8]Bristol-Myers Squibb, Redwood City, CA, USA; [9]Current affiliation: Vir Biotechnology, San Francisco, CA; [10]Department of Genetics & Development, Columbia University, New York, NY, USA;

[11]Herbert Irving Comprehensive Cancer Center, Columbia University, New York, NY, USA; [12]Department of Medicine, Division of Hematology/Oncology, Columbia University, New York, NY, USA.

Summary

Immunotherapy is a treatment for many types of cancer, primarily due to deep and durable clinical responses mediated by immune checkpoint blockade (ICB)[1,2]. Prostate cancer is a notable exception in that it is generally unresponsive to ICB. The standard treatment for advanced prostate cancer is androgen-deprivation therapy (ADT), a form of castration (CTX). ADT is initially effective, but over time patients eventually develop castration-resistant prostate cancer (CRPC). Here, we focused on defining tumor-cell intrinsic factors that contribute to prostate cancer progression and resistance to immunotherapy. We analyzed cancer cells isolated from castration-sensitive and castration-resistant prostate tumors, and discovered that castration resulted in significant secretion of Interleukin-8 (IL-8) and it's likely murine homolog Cxcl15. These chemokines drove subsequent intra-tumoral infiltration with polymorphonuclear myeloid-derived suppressor cells (PMN-MDSCs), promoting tumor progression. PMN-MDSC infiltration was abrogated when IL-8 was deleted from prostate cancer epithelial cells using CRISPR/Cas9, or when PMN-MDSC migration was blocked with antibodies against the IL-8 receptor CXCR2. Blocking PMN-MDSC infiltration in combination with anti-CTLA-4 delayed the onset of castration resistance and increased the density of polyfunctional CD8 T cells in tumors. Taken together, our findings establish castration-mediated IL-8 secretion and subsequent PMN-MDSC infiltration as a key suppressive mechanism in the

progression of prostate cancer. Targeting of the IL-8/CXCR2 axis around the time of ADT, in combination with ICB, represents a novel therapeutic approach to delay prostate cancer progression to advanced disease.

Main

After primary therapy with surgery or radiation, approximately 40% of prostate cancer patients develop progressive disease. The standard treatment for recurrent prostate cancer is androgen-deprivation therapy (ADT), but the majority of these patients eventually develop castration-resistance (CR). Although some patients with metastatic castration-resistant prostate cancer (mCRPC) benefit from the cancer vaccine sipuleucel-T[3], neither CTLA-4 blockade[4,5] nor PD-1 blockade[6] has reliably produced meaningful clinical responses. Potential reasons for this include a low total mutational burden (TMB) as well as poor infiltration by CD8 T cells[7].

We and others have shown that ADT initially increases CD8 T cell infiltration into prostate tumors[8-10], and this response is augmented pre-clinically with anti-CTLA-4[11]. Emerging data suggest that immune-resistance in prostate cancer involves dysfunctional myeloid cells known as myeloid-derived suppressor cells (MDSCs) in the tumor microenvironment (TME)[12,13]. MDSCs secrete IL-23, which acts directly on prostate cancer epithelial cells to drive castration-resistance[14]. Importantly, the mechanism(s) by which suppressive MDSCs are recruited to the prostate TME are largely unknown.

To identify immune-related tumor-cell intrinsic factors involved in prostate cancer progression, we performed expression analyses on murine prostate cancer cells pre- and

post- castration. We used the MCRedAL prostate cancer cell line; an RFP expressing version of the Myc-Cap cell line characterized by *MYC* overexpression[15]. Like human prostate cancer, MCRedAL tumors are initially castration-sensitive (CS), but castration-resistance (CR) develops approximately 30 days after castration (Extended Data Fig. 1a). Pre- and post- ADT tumor cells were sorted to > 96% purity (Extended Data Fig. 1b) and analyzed (Fig. 1a-b and Extended Data Fig. 1c). A number of cytokine and chemokine transcripts were significantly up-regulated post-ADT (Fig. 1b right), including *Cxcl15*, a CXC chemokine with a conserved ELR motif (Extended Data Table 1), which is the likely murine homolog of human *IL-8* (*CXCL8*)[16-19]. qRT-PCR and ELISA assays confirmed the upregulation of Cxcl15 post-ADT at the protein level (Extended Data Fig. 1d). In addition to the chemokines above, GSEA revealed the upregulation of several pro-inflammatory pathways post-ADT (Fig. 1c). *In vitro* experiments using the human androgen-responsive LNCaP cell line corroborated a role for these pro-inflammatory signals, showing that in the absence of androgen, TNFα upregulated IL-8 expression in a dose-dependent manner (Fig. 1d left); while AR signaling in the absence of inflammation did not affect IL-8 expression (Fig. 1d right). These data led to the hypothesis that AR signaling directly suppresses *IL-8* expression in prostate cancer cells. We performed *in silico* ChIP-Seq analyses using human LNCaP cells (GSE83860) and found AR binding at the *IL-8* promoter in the presence of the potent androgen dihydrotestosterone (DHT; Fig. 1e top). This androgen dependent binding was verified by ChIP-qRT-PCR (Fig. 1f).

To further explore the role of AR in IL-8 regulation, we interrogated RNA polymerase binding and transcription marks found at sites of active promoters[20]. In the presence of DHT, binding of RNA polymerase II (pol II), phosphorylated serine 2 RNA polymerase II

89 (pSer2 pol II) and histone H3 tri-methyl Lys4 (H3K4me3) to the IL-8 locus were
90 substantially reduced, consistent with reduced transcriptional activity (Fig. 1f).
91 Conversely, pSer2 pol II binding to the promoter of the well-established AR-regulated
92 gene *PSA* (*KLK3*), was significantly increased in the presence of DHT as expected
93 (Extended Data Fig. 1e). Consistent with a role for inflammation, TNFα significantly
94 increased p65 binding at the *IL-8* (*CXCL8*) promoter in LNCaP cells (Fig. 1e bottom). No
95 significant binding of AR was detected at the promoters of the chemokines *CXCL1*,
96 *CXCL2*, *CXCL5* or *CXCL12* (Extended Data Fig. 1f). These data suggest that AR directly
97 suppresses *IL-8* expression through repressive AR binding to the *IL-8* promoter. Taken
98 together, we found that IL-8 transcription is up-regulated by pro-inflammatory signaling,
99 and down-regulated by AR signaling (Fig. 1g).

100 We next investigated the effects of ADT on the expression of *Cxcl15 in vivo*, using RNA
101 in situ hybridization (RISH) to study Myc-Cap tumors. We found that CR tumors
102 expressed increased *Cxcl15* as compared to CS tumors, particularly in epithelial
103 (PanCK$^+$) tumor cells (Fig. 2a, Extended Data Fig. 2a). These findings were confirmed *in*
104 *vitro*, both at the mRNA and protein level (Fig. 2b). To investigate these findings in the
105 context of human prostate cancer, we used three paired cell lines in which isogenic CR
106 lines were derived from CS progenitors. For each pair, the CR line expressed significantly
107 increased IL-8 as compared to the CS counterpart, both at the mRNA and protein level
108 (Fig. 2c-d). This observation held across a panel of AR expressing prostate cancer cell
109 lines; with higher levels of *IL-8* expression in cell lines from castration-resistant disease
110 (Extended Data Fig. 2b). To test whether AR modulates *Cxcl15* expression in <u>benign</u>
111 prostate epithelium, we used RISH to study WT mice treated with ADT, and WT mice

112 treated with ADT followed by testosterone (T) repletion (Extended Data Fig. 2c). These
113 data (Fig. 2e-f) showed increased epithelial *Cxcl15* expression in ADT samples with
114 expression significantly decreased by testosterone repletion (Fig. 2f). This observation
115 was further corroborated by interrogating a dataset (GSE8466) profiling human prostate
116 epithelial cells isolated by laser-capture microdissection (LCM) from men undergoing ADT
117 and ADT with testosterone supplementation. Testosterone repletion significantly reduced
118 *IL-8* mRNA expression (Fig. 2g), supporting the hypothesis that AR signaling down-
119 regulates IL-8 expression. In agreement with these data from benign prostate tissues, we
120 LCM-enriched tumor prostate epithelium from high-risk PCa patients treated with ADT on
121 a neo-adjuvant trial (NCT01696877) and found increased *IL-8* expression as compared
122 to tumors from age and stage-matched untreated controls (Fig. 2h). Taken together,
123 analyses using human tissues strongly support the notion that castration increases *IL-8*
124 expression in prostate epithelial cells.

125 We next quantified castration-mediated immune infiltration in Myc-Cap allografts (Fig. 3a).
126 Consistent with prior data[11], ADT promoted a transient T cell influx, without significant
127 changes in tumor associated macrophage (TAM) populations (Fig. 3b). By contrast,
128 PMN-MDSC infiltration was significantly increased in CR tumors (Fig. 3b), as verified by
129 IHC (Fig. 3c). We found similar results in human prostate cancer xenografts (Extended
130 Data Fig. 3a-b). PMN-MDSC infiltration also increased in WT mice treated with ADT, but
131 not in WT mice treated with ADT then repleted with testosterone (Extended Data Fig. 3c),
132 supporting a causal relationship between ADT and PMN-MDSC infiltration. Molecular
133 profiling of the infiltrating myeloid cells revealed a signature consistent with functional

134 PMN-MDSCs, including up-regulation of *IL-1b*, *Arg2* and *IL-23a*[14] (Fig. 3d; Extended Data
135 Table 2). In particular, increased expression of *IL-23a* and *Cxcr2* was verified by qRT-
136 PCR (Fig. 3e) and flow cytometry (Extended Data Fig. 3d). To test whether blocking the
137 IL-8/CXCR2 axis was sufficient to attenuate post-ADT PMN-MDSC infiltration, we treated
138 prostate-tumor bearing mice with anti-CXCR2 and found that blocking CXCR2
139 significantly diminished tumor infiltration with PMN-MDSCs in both human (PC3) and
140 murine (Myc-Cap) immunodeficient and immunocompetent models (Fig. 3f and Extended
141 Data Fig. 3e-f). To confirm this observation at the genetic level, we used CRISPR/Cas9
142 to generate human (PC3) and mouse (Myc-Cap) lines that were knocked out for human
143 IL-8 or the murine IL-8 homolog Cxcl15, respectively. We observed a clear decrease in
144 PMN-MDSC infiltration in both settings (Fig. 3g and Extended Data Fig. 3e-f).

145 We next asked whether the supernatants from castration-resistant MCRedAL (CR-
146 MCRedAL) cells were sufficient to drive PMN-MDSC migration *in vitro*. In line with *in vivo*
147 results (Fig. 3f-g and Extended Data Fig. 4a-c), we found that PMN-MDSC migrated
148 towards the supernatant of CR tumors and migration was significantly attenuated by
149 CXCR2 blockade (Extended Data Fig. 4d). Human prostate cancer (PC3) showed an
150 identical pattern. To confirm a role for IL-8 in PMN-MDSC migration, we generated IL-8
151 KO CR-LNCaP (LNCaP-abl) using CRISPR/Cas9. Supernatants from IL-8 KO cells were
152 significantly attenuated in their ability to promote PMN-MDSC migration (Extended Data
153 Fig. 4e). These PMN-MDSCs were functional and suppressed CD8 T cell proliferation in
154 a dose-dependent manner (Extended Data Fig. 4f-i). Although CXCR2 blockade
155 decreased PMN-MDSC migration, it did not significantly alter their suppressor function

156 (Extended Data Fig. 4j). Similarly, Cxcl15 loss did not diminish the suppressive function
157 of PMN-MDSCs (Extended Data Fig. 4k). Taken together these findings reinforce a
158 functional role for castration-mediated IL-8 secretion in PMN-MDSC migration.

159 Finally, we investigated the pre-clinical activity of blocking the IL-8/CXCR2 axis at the time
160 of androgen-deprivation in the Myc-Cap model. Notably, in the absence of
161 immunotherapy the combination of ADT and CXCR2 blockade was not effective
162 (Extended Data Fig. 5a). In contrast, combining CXCR2 blockade with ICB (anti-CTLA-
163 4; Fig. 4a) resulted in significantly increased survival (Fig. 4b). This triple combination
164 (ADT + anti-CXCR2 + anti-CTLA-4) was effective even when tumors were relatively
165 advanced (400 mm^3) at the time of treatment (Extended Data Fig. 5b&d). Macrophage
166 modulation with anti-CSF1R was not effective therapeutically in this setting (Extended
167 Data Fig. 5c&e). Mechanistically, the increased anti-tumor effects mediated by the
168 addition of anti-CXCR2 to ADT + anti-CTLA-4 did not appear to be due to increased T cell
169 infiltration (Fig. 4c and Extended Data Fig. 5f-h), nor due to decreased Treg infiltration
170 (Fig. 4d), but rather correlated with an increase in polyfunctional effector CD8 T cells in
171 tumor-draining lymph nodes (TDLN) and spleens (Fig. 4e&f).

172 In summary, these studies showed that castration mediates increased IL-8 secretion by
173 prostate cancer epithelial cells by releasing AR-mediated transcriptional repression. IL-8
174 (and Cxcl15) up-regulation then drives prostate tumor infiltration with PMN-MDSCs. We
175 found that blocking CXCR2 at the time of androgen-deprivation therapy attenuates PMN-
176 MDSC infiltration, rendering prostate tumors more responsive to ICB. It is noteworthy
177 that in other murine models the recruitment of PMN-MDSC and neutrophils may be driven

178 by other chemokines, including Cxcl1[21] and Cxcl12[22]. Our findings are corroborated by
179 clinical data showing that PMN-MDSCs accumulate in the blood of patients with advanced
180 prostate cancer[23-25], and that an intratumoral PMN signature is associated with poor
181 outcome[26]. Our data are also supported by pre-clinical studies showing that blocking
182 MDSC function increases the efficacy of ICB in animal models of CRPC[12]. Consistent
183 with recent data, we found that the PMN-MDSCs infiltrating prostate tumors express IL-
184 23[14]. We further showed that inhibiting the recruitment of these cells peri-castration
185 augmented the CD8 T cell effector function initiated by ICB. Based on these findings, we
186 have initiated a phase 1b/2 trial (NCT03689699) to test whether adding ICB and anti-IL-
187 8 to a short course of ADT can prevent PMN-MDSC infiltration and delay progression in
188 men with castration-sensitive prostate cancer. In summary, targeting the IL-8/CXCR2
189 pathway following ADT in combination with immune checkpoint blockade may represent
190 a novel treatment paradigm to improve responses to immunotherapy and delay the onset
191 of castration-resistance.
192

193 **Acknowledgments**

194 We thank members of the Drake Lab for discussion and insightful comments; F. Veglia
195 for advice with *in vitro* suppression assays; K.C. Smith, A. Floratos, and the Center for
196 Computational Biology and Bioinformatics at Columbia University for ChIP-Seq analysis;
197 S. Coley, T. Swayne, E. Munteanu, and the Confocal and Specialized Microscopy Shared
198 Resource at Columbia University for help with microscopy; L. Dasko-Vincent from the
199 Sidney Kimmel Comprehensive Cancer Center Imaging Facility at Johns Hopkins for
200 support with LCM, J. Pevsner for assistance on protein homology analyses, and B.

Johnson for help with statistical analyses. This study was supported by U.S. Department of Defense (W81XWH-13-1-0369), U.S. National Institutes of Health National Cancer Institute (R01: CA127153), the Patrick C. Walsh Fund, the OneInSix Foundation, and the Prostate Cancer Foundation. Research reported in this publication was performed in the CCTI Flow Cytometry Core, supported in part by the Office of the Director, National Institutes of Health under awards S10OD020056. H&E/IHC staining and image collection for this work was performed in the Molecular Pathology Shared Resource and the Confocal and Specialized Microscopy Shared Resource of the Herbert Irving Comprehensive Cancer Center at Columbia University, supported by NIH grant #P30 CA013696 (National Cancer Institute). The content is solely the responsibility of the authors and does not necessarily represent the official views of the National Institutes of Health.

Author contributions

Z.A.L.B., M.C.H., M.G.C., N.C., N.J.V., and A.O. performed experiments; C.H., J.J., C.J.B., P.J.H., M.J.S., and A.J.K. contributed essential reagents; Z.A.L.B., M.C.H., A.M.C. and C.G.D. designed and supervised experiments; M.C.H., K.S.S., and A.D.M. coordinated the study on human samples; C.G.D. supervised the study. Z.A.L.B. and C.G.D. wrote the manuscript, which was edited by all authors.

Author information

C.G.D. has stock or ownership interests in Compugen, Harpoon, Kleo, Potenza, and Tizona Therapeutics, and has served as a consultant for Agenus, Dendreon, Janssen

224 Oncology, Eli Lilly, Merck, AstraZeneca, MedImmune, Pierre Fabre, Genentech, and
225 Genocea Biosciences. A.M.C. is a shareholder of Aclaris Therapeutics, Inc, and a
226 consultant for Dermira, Inc. and Aclaris Therapeutics, Inc. Columbia University has filed
227 a US patent claiming the benefit of U.S. Provisional Patent Application No. 62/809,060
228 (inventors C.G.D. and Z.A.L.B.) on the use of IL-8/CXCR2 blockade of PMN-MDSC
229 recruitment to the TME for the treatment of prostate cancer. The remaining authors
230 declare no competing financial interest.

231 Correspondence and request for materials should be addressed to C.G.D.
232 (cgd2139@cumc.columbia.edu).

233

234 **Data Availability**

235 The data that support the findings of this study are available from the corresponding
236 author upon reasonable request.

237

238 **Biological Materials**

239 Biological materials used in this study may be requested from the corresponding
240 author, with the exception of anti-CTLA-4 and anti-CXCR2 antibodies which were
241 obtained through an MTA with A.K and M.S.

242 **Figures**

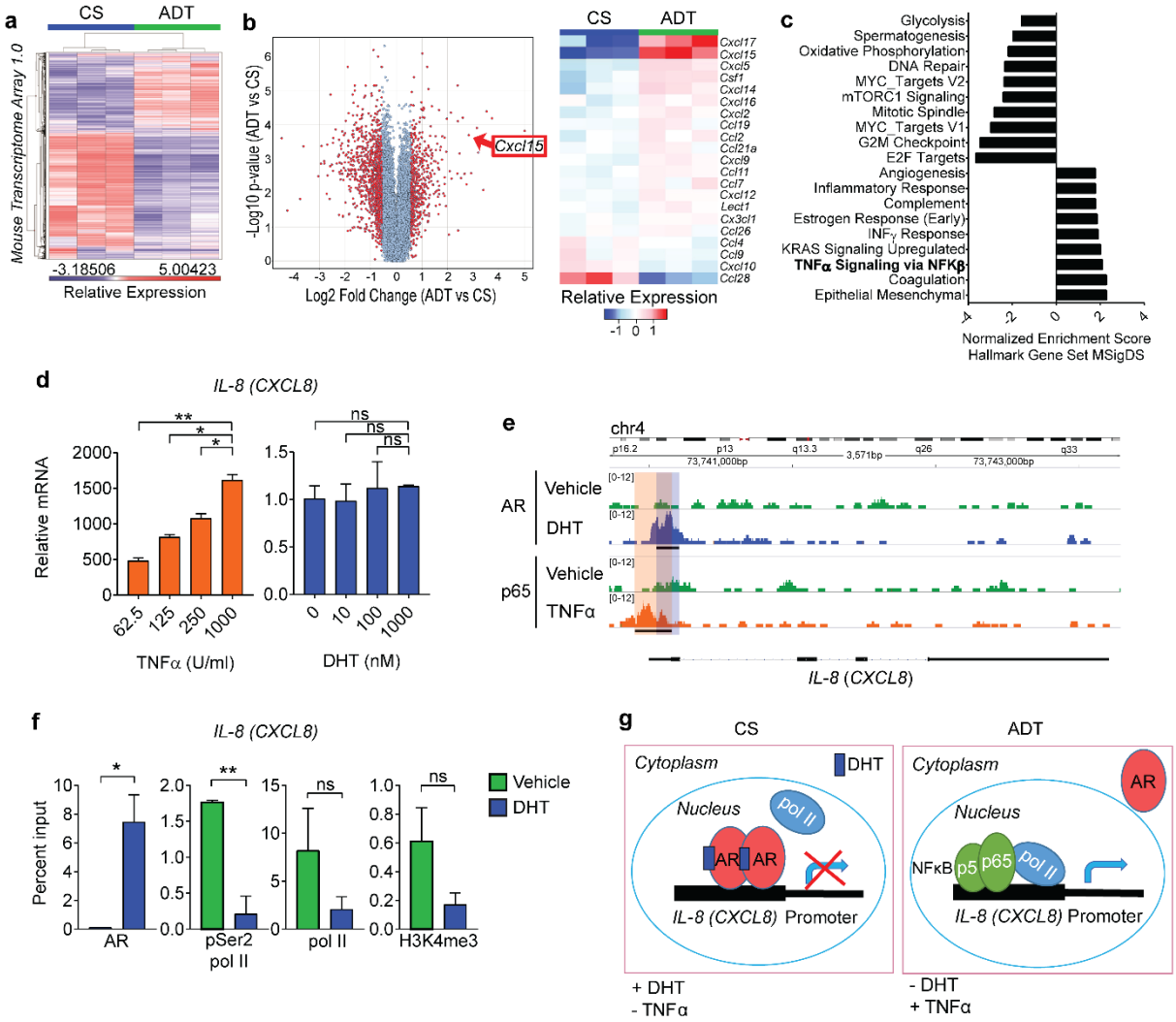

243

244 **Figure 1 | Androgen-Deprivation Therapy (ADT) Increases IL-8 Expression in**
245 **Prostate Cancer Cells. a,** Differential expression profile of tumor epithelial cells isolated
246 from castration-sensitive (CS) and ADT-treated MCRedAL tumor bearing mice. Heatmap
247 showing transcripts 3 standard deviations away from the mean (n = 3 per group). **b,**
248 Differential chemokine expression of tumor epithelial cells isolated from CS and ADT
249 tumor bearing mice (replicate numbers as in **a**). Left, volcano plot showing gene

250 expression among all MTA 1.0 microarray transcripts. Right, heatmap of normalized
251 chemokine transcripts. **c,** Hallmarks gene sets pathway analysis post-ADT shows NF-κB
252 up-regulation post-ADT. **d,** qRT-PCR quantification of *IL-8* in LNCaP cells cultured at
253 indicated concentrations of TNFα and DHT, cells cultured in androgen-free media as
254 described in materials and methods (n = 3 per condition, repeated x 2). Expression levels
255 normalized to mean ΔCT level in samples cultured in androgen free media without TNFα
256 or DHT. **e,** ChIP-Seq analysis of AR at the *IL-8* (*CXCL8*) promoter in LNCaP cells cultured
257 in the presence of either vehicle (DMSO), DHT (100 nM), or TNFα (1000 U/ml) (n = 2 per
258 group; GSE83860). **f,** ChIP quantitative RT-PCR (qRT-PCR) analysis of AR, pSer2 Pol
259 II, pol II, and H3K4me3 at the *IL-8* (*CXCL8*) promoter (n = 3 per group). Transfected
260 LNCaP cells treated for 24 hours with or without DHT (100 nM). **g,** Schematic model of
261 the interplay between AR and NFkB in the regulation of IL-8 transcription. For **e**, loci with
262 significant differential binding (black bar) were identified as described in materials and
263 methods. Error bars represent standard error. Unpaired t-tests were performed, *p*-values
264 ≤ 0.05 (*), 0.01 (**), 0.001 (***) and 0.0001 (****); *p*-values ≥ 0.05 (ns).

265

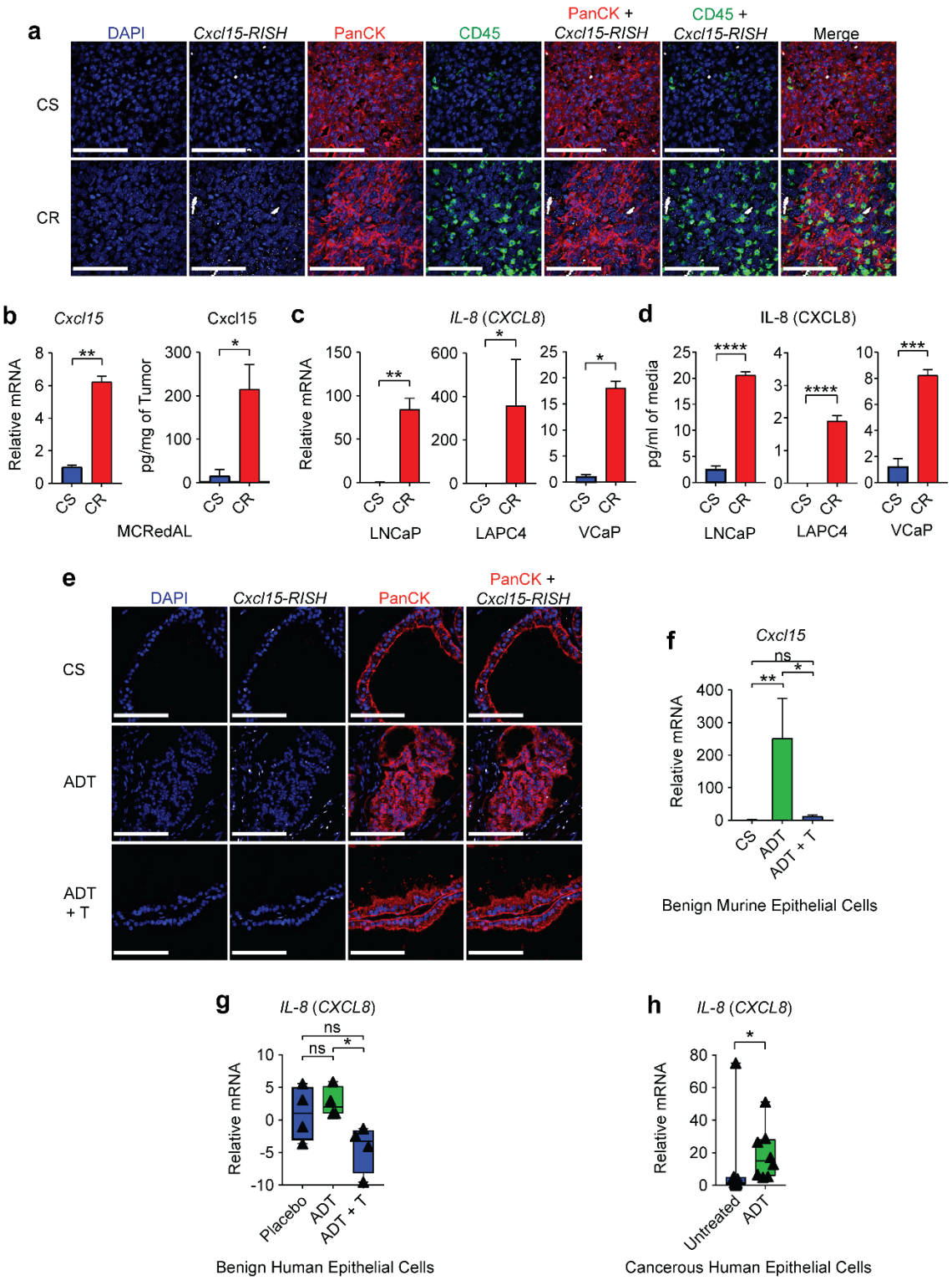

Figure 2 | IL-8 is Up-Regulated in Post-Castration and Castration-Resistant Prostate Cancer Cells. **a,** Representative images of *Cxcl15* fluorescent detection (murine

269 homologue of IL-8) in Myc-Cap tumors. Tumors were harvested when volumes reached
270 ~500mm^3 (CS group), 7 days after androgen-deprivation (ADT), or at the time of
271 castration-resistance (CR) and hybridized with CF568-labeled probe sets (white) to
272 *Cxcl15*, CF640-labeled anti-PanCK antibody (red), and CF488-labeled anti-CD45
273 antibody (green). Nuclei counterstained with DAPI (blue). Repeated x 3. **b,** Gene and
274 protein expression of Cxcl15 in MCRedAL cells of indicated tumor samples by qRT-PCR
275 and ELISA, respectively (n = 3 per group, repeated x 2). **c,** qRT-PCR quantification of *IL-*
276 *8* in human AR positive castration-sensitive cells (CS: LNCaP, LAPC4, and VCaP) and
277 their castration-resistant counterparts (CR: LNCaP-abl, LAPC4-CR, and VCaP-CR),
278 replicate numbers as in **b**. **d,** IL-8 protein expression in the isogenic cell pairs from **c**
279 quantified by ELISA, replicate numbers as in **c**. **e,** Representative images of *Cxcl15*
280 fluorescent detection in benign murine prostate tissue samples from castration-sensitive
281 (CS), androgen-deprivation treated (ADT), and ADT-treated mice that received
282 testosterone repletion (ADT + T). Tissue sections hybridized with CF568-labeled probe
283 sets (white) to *Cxcl15*, and CF640-labeled anti-PanCK antibody (red). Nuclei were
284 counterstained with DAPI (blue). Repeated x 3. **f,** qRT-PCR analysis of *Cxcl15*
285 expression in prostate luminal epithelial cells from indicated treatment groups (n = 3 per
286 group). Prostate luminal epithelial cells were isolated based on their
287 GFP$^+$CD49f^{int}CD24$^+$CD45$^-$F4/80$^-$CD11b$^-$ expression by flow sorting into Trizol LS. **g,**
288 Expression of *IL-8* in human prostate epithelial cells micro-dissected from patients in a
289 clinical trial (NCT00161486) receiving placebo, androgen-deprivation treatment (ADT), or
290 ADT plus testosterone repletion (ADT + T). Z-score values of microarray transcripts from
291 benign prostate biopsies were normalized to placebo samples (n = 4 per group;

292 GSE8466). **h,** Expression of *IL-8* in human prostate cancer epithelial cells micro-
293 dissected from untreated or ADT-treated (NCT01696877; n = 8 per group) patients as
294 determined by qRT-PCR. RISH images are at 60X magnification; scale bar = 100 μm.
295 Gene expression levels were normalized to the mean ΔCT level in samples from CS,
296 untreated or placebo groups. For **b-g**, unpaired t-tests were performed; for **h** a Mann-
297 Whitney U test was used due to the non-normal data distribution observed. *p*-values ≤
298 0.05 (*) and 0.01 (**); *p*-values ≥ 0.05 (ns) shown. The range in box and whiskers plots
299 shows min and max values such that all data are included.
300

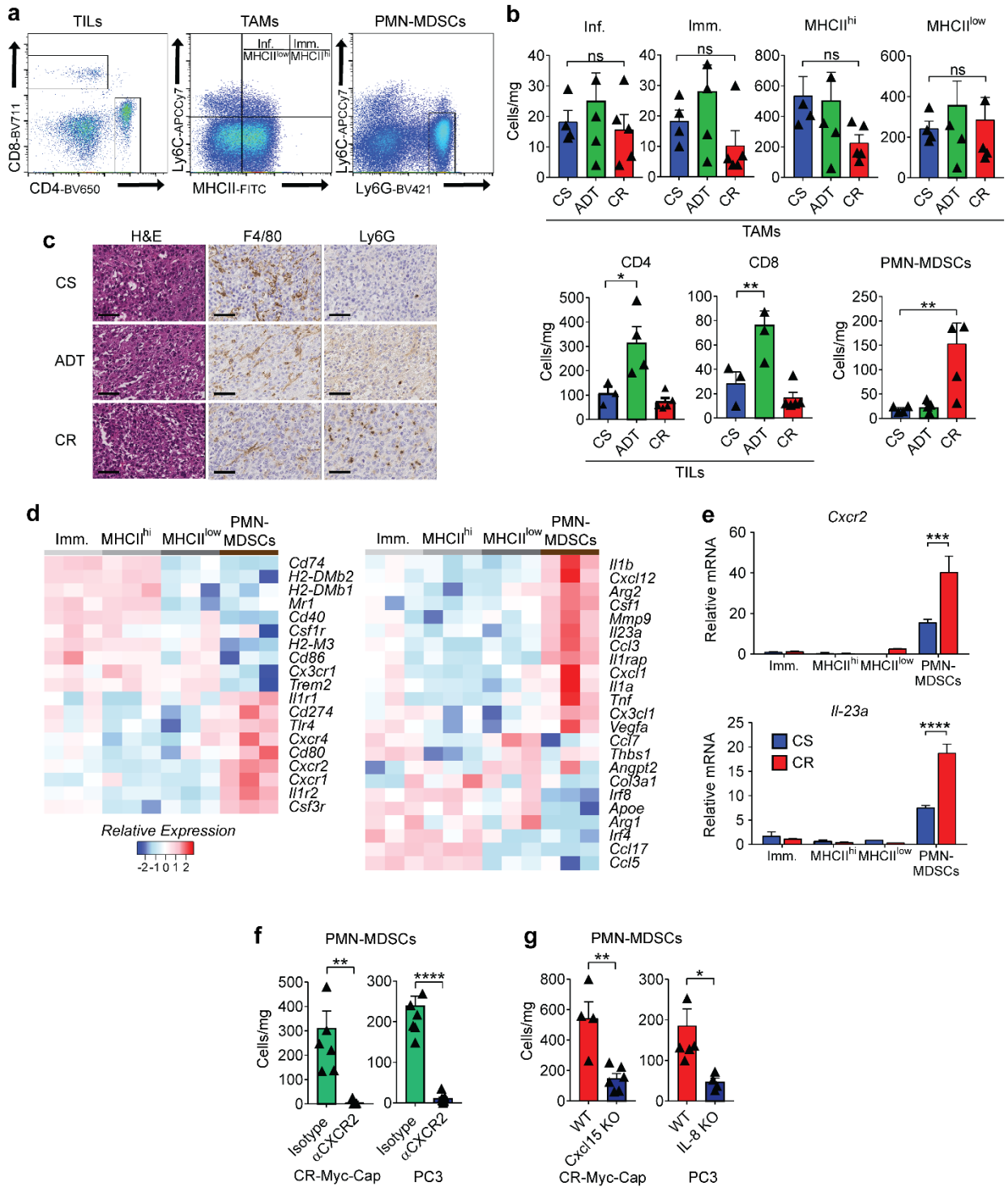

Figure 3 | Castration-mediated IL-8 Up-Regulation Promotes PMN-MDSC Infiltration. a, Gating strategy used to profile the immune compartment of the TME by

304 flow cytometry. Tumor associated macrophages (TAMs) gated based on $CD45^+Ly6G^-$
305 $F4/80^+CD11b^+$, Inflammatory (Inf.) TAMs as $CD45^+CD11b^+F4/80^+Ly6C^+MHCII^-$, immature
306 (Imm.) TAMs as $CD45^+CD11b^+F4/80^+Ly6C^+MHCII^+$, $MHCII^{hi}$ TAMs as
307 $CD45^+CD11b^+F4/80^+Ly6C^-MHCII^+$, $MHCII^{low}$ TAMs as $CD45^+CD11b^+F4/80^+Ly6C^-MHCII^-$,
308 tumor Infiltrating Lymphocytes (TILs) $CD45^+CD4^+$ or $CD45^+CD8^+$, tumor infiltrating
309 polymorphonuclear myeloid-derived suppressor cells (PMN-MDSCs) as
310 $CD45^+CD11b^+Ly6C^+Ly6G^+$. **b,** TAM, TIL, and PMN-MDSC density normalized to mg of
311 tumor weight (cells/mg; n ≥ 3 per group, repeated x 2). **c,** Representative H&E and
312 immunohistochemistry (F4/80 and Ly6G) of indicated murine allografts (repeated x 3). **d,**
313 Normalized expression of selected genes determined by NanoString nCounter gene
314 analysis in sorted myeloid fractions defined as in **a** (n = 3 per group). **e,** qRT-PCR
315 quantification of *Cxcr2* and *Il-23* in indicated populations of Myc-Cap tumors (n = 3 per
316 group). **f** and **g,** Density of PMN-MDSCs normalized to mg of tumor weight (cells/mg) in
317 Myc-Cap and PC3 tumors (n ≥ 4 per group, repeated x 2). Cells quantified by flow
318 cytometry as in **a**, tumors implanted and harvested as in materials and methods. H&E
319 and IHC images at 40X magnification; scale bar = 50 μm. Gene expression levels
320 normalized to the mean ΔCT level in samples from the Immature TAMs (Imm.) group.
321 Unpaired t-tests performed, *p*-values ≤ 0.05 (*), 0.01 (**), 0.001 (***) and 0.0001 (****); *p*-
322 values ≥ 0.05 (ns).

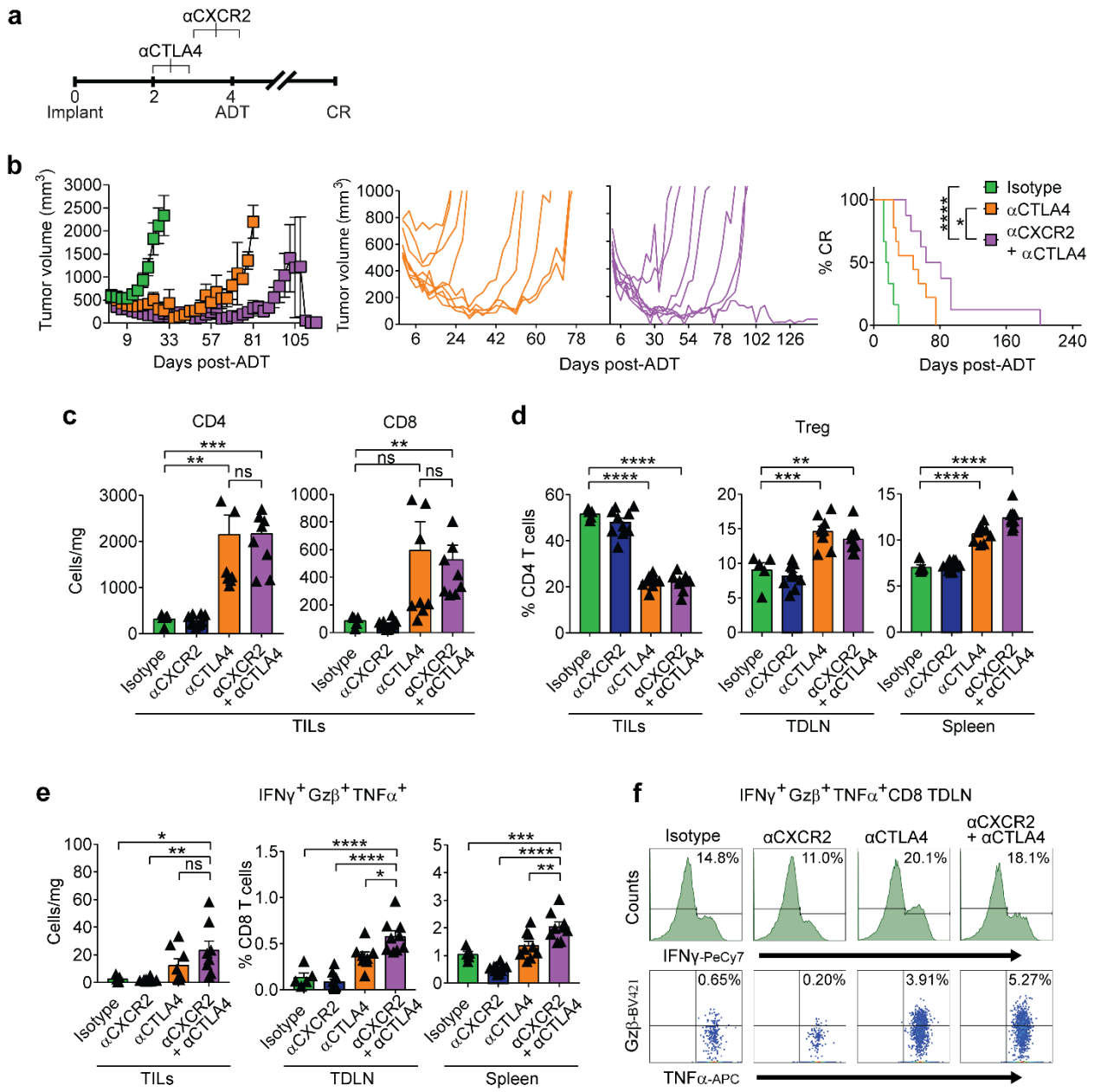

Figure 4 | CXCR2 Blockade Improves Response to Immune Checkpoint Blockade Following Androgen-Deprivation Therapy. **a,** Treatment scheme, scale = weeks. Animals sacrificed for immune phenotyping 1 week post-ADT. **b,** Tumor growth and survival curves of mice from isotype vs. anti-CTLA-4 vs. anti-CTLA-4 + anti-CXCR2 groups treated as described in **a** (black line vs. orange line vs. purple line, respectively; n

329 ≥ 8 per group, repeated x 2). **c,** Tumor infiltrating lymphocyte (TILs) density in indicated
330 treatment groups (n ≥ 5 per group, repeated x 2). **d,** Treg percentages (as fraction of
331 CD4) in indicated tissues (n ≥ 5 per group, repeated x 2). **e,** Polyfunctional CD8 T cells,
332 left panel = density, center/right panels = percentage of total CD8, animals numbers as in
333 **d**. **f,** Representative histograms and dot plots of polyfunctional $CD8^+$ $IFN\gamma^+Gz\beta^+TNF\alpha^+$
334 from tumor draining lymph nodes (TDLN). Repeated x 2. For **a-f**, treatment was initiated
335 when tumor volumes reached $200mm^3$. Average tumor volume (±s.e.m.) for each
336 experimental group. Wilcoxon test used for survival analysis. Flow cytometry as in
337 materials and methods. Unpaired t-tests performed, *p*-values ≤ 0.05 (*), 0.01 (**), 0.001
338 (***) and 0.0001 (****); *p*-values ≥ 0.05 (ns).
339
340
341
342
343
344
345
346
347
348
349
350
351

352 **References**

353 1 Topalian, S. L., Drake, C. G. & Pardoll, D. M. Immune checkpoint blockade: a
354 common denominator approach to cancer therapy. *Cancer Cell* **27**, 450-461,
355 doi:10.1016/j.ccell.2015.03.001 (2015).

356 2 Drake, C. G. Prostate cancer as a model for tumour immunotherapy. *Nat Rev*
357 *Immunol* **10**, 580-593, doi:10.1038/nri2817 (2010).

358 3 Kantoff, P. W. *et al.* Sipuleucel-T immunotherapy for castration-resistant prostate
359 cancer. *N Engl J Med* **363**, 411-422, doi:10.1056/NEJMoa1001294 (2010).

360 4 Kwon, E. D. *et al.* Ipilimumab versus placebo after radiotherapy in patients with
361 metastatic castration-resistant prostate cancer that had progressed after docetaxel
362 chemotherapy (CA184-043): a multicentre, randomised, double-blind, phase 3
363 trial. *Lancet Oncol* **15**, 700-712, doi:10.1016/S1470-2045(14)70189-5 (2014).

364 5 Beer, T. M. *et al.* Randomized, Double-Blind, Phase III Trial of Ipilimumab Versus
365 Placebo in Asymptomatic or Minimally Symptomatic Patients With Metastatic
366 Chemotherapy-Naive Castration-Resistant Prostate Cancer. *J Clin Oncol* **35**, 40-
367 47, doi:10.1200/JCO.2016.69.1584 [pii]
368 10.1200/JCO.2016.69.1584 (2017).

369 6 Topalian, S. L. *et al.* Safety, activity, and immune correlates of anti-PD-1 antibody
370 in cancer. *N Engl J Med* **366**, 2443-2454, doi:10.1056/NEJMoa1200690 (2012).

371 7 Gao, J. *et al.* VISTA is an inhibitory immune checkpoint that is increased after
372 ipilimumab therapy in patients with prostate cancer. *Nat Med* **23**, 551-555,
373 doi:10.1038/nm.4308 (2017).

374 8 Mercader, M. *et al.* T cell infiltration of the prostate induced by androgen withdrawal
375 in patients with prostate cancer. *Proc Natl Acad Sci U S A* **98**, 14565-14570,
376 doi:10.1073/pnas.251140998 (2001).
377 9 Gannon, P. O. *et al.* Characterization of the intra-prostatic immune cell infiltration
378 in androgen-deprived prostate cancer patients. *J Immunol Methods* **348**, 9-17,
379 doi:10.1016/j.jim.2009.06.004 (2009).
380 10 Drake, C. G. *et al.* Androgen ablation mitigates tolerance to a prostate/prostate
381 cancer-restricted antigen. *Cancer Cell* **7**, 239-249, doi:10.1016/j.ccr.2005.01.027
382 (2005).
383 11 Shen, Y. C. *et al.* Combining intratumoral Treg depletion with androgen deprivation
384 therapy (ADT): preclinical activity in the Myc-CaP model. *Prostate Cancer Prostatic*
385 *Dis* **21**, 113-125, doi:10.1038/s41391-017-0013-x (2018).
386 12 Lu, X. *et al.* Effective combinatorial immunotherapy for castration-resistant
387 prostate cancer. *Nature* **543**, 728-732, doi:10.1038/nature21676 (2017).
388 13 Lopez-Bujanda, Z. & Drake, C. G. Myeloid-derived cells in prostate cancer
389 progression: phenotype and prospective therapies. *J Leukoc Biol* **102**, 393-406,
390 doi:10.1189/jlb.5VMR1116-491RR (2017).
391 14 Calcinotto, A. *et al.* IL-23 secreted by myeloid cells drives castration-resistant
392 prostate cancer. *Nature* **559**, 363-369, doi:10.1038/s41586-018-0266-0 (2018).
393 15 Watson, P. A. *et al.* Context-dependent hormone-refractory progression revealed
394 through characterization of a novel murine prostate cancer cell line. *Cancer Res*
395 **65**, 11565-11571, doi:10.1158/0008-5472.CAN-05-3441 (2005).

396 16 Hol, J., Wilhelmsen, L. & Haraldsen, G. The murine IL-8 homologues KC, MIP-2,
397 and LIX are found in endothelial cytoplasmic granules but not in Weibel-Palade
398 bodies. *J Leukoc Biol* **87**, 501-508, doi:10.1189/jlb.0809532 (2010).
399 17 Rossi, D. L. *et al.* Lungkine, a novel CXC chemokine, specifically expressed by
400 lung bronchoepithelial cells. *J Immunol* **162**, 5490-5497 (1999).
401 18 Schmitz, J. M., McCracken, V. J., Dimmitt, R. A. & Lorenz, R. G. Expression of
402 CXCL15 (Lungkine) in murine gastrointestinal, urogenital, and endocrine organs.
403 *J Histochem Cytochem* **55**, 515-524, doi:10.1369/jhc.6A7121.2007 (2007).
404 19 Chen, R. *et al.* Telomerase Deficiency Causes Alveolar Stem Cell Senescence-
405 associated Low-grade Inflammation in Lungs. *J Biol Chem* **290**, 30813-30829,
406 doi:10.1074/jbc.M115.681619 (2015).
407 20 Karlic, R., Chung, H. R., Lasserre, J., Vlahovicek, K. & Vingron, M. Histone
408 modification levels are predictive for gene expression. *Proc Natl Acad Sci U S A*
409 **107**, 2926-2931, doi:10.1073/pnas.0909344107 (2010).
410 21 Kumar, V. *et al.* Cancer-Associated Fibroblasts Neutralize the Anti-tumor Effect of
411 CSF1 Receptor Blockade by Inducing PMN-MDSC Infiltration of Tumors. *Cancer*
412 *Cell* **32**, 654-668 e655, doi:10.1016/j.ccell.2017.10.005 (2017).
413 22 Patnaik, A. *et al.* Cabozantinib Eradicates Advanced Murine Prostate Cancer by
414 Activating Antitumor Innate Immunity. *Cancer Discov* **7**, 750-765,
415 doi:10.1158/2159-8290.CD-16-0778 (2017).
416 23 Kawahara, T. *et al.* Neutrophil-to-lymphocyte ratio predicts prostatic carcinoma in
417 men undergoing needle biopsy. *Oncotarget* **6**, 32169-32176,
418 doi:10.18632/oncotarget.5081 (2015).

419 24 Yin, X. *et al.* Prognostic Role of Neutrophil-to-Lymphocyte Ratio in Prostate
420 Cancer: A Systematic Review and Meta-analysis. *Medicine (Baltimore)* **95**, e2544,
421 doi:10.1097/MD.0000000000002544 (2016).
422 25 Alfaro, C. *et al.* Tumor-Produced Interleukin-8 Attracts Human Myeloid-Derived
423 Suppressor Cells and Elicits Extrusion of Neutrophil Extracellular Traps (NETs).
424 *Clin Cancer Res* **22**, 3924-3936, doi:10.1158/1078-0432.CCR-15-2463 (2016).
425 26 Gentles, A. J. *et al.* The prognostic landscape of genes and infiltrating immune
426 cells across human cancers. *Nat Med* **21**, 938-945, doi:10.1038/nm.3909 (2015).
427
428
429
430
431
432
433
434
435
436
437
438
439
440
441

442 **Materials and Methods**

443 *Patient Samples*

444 Formalin fixed, paraffin embedded (FFPE) human prostate cancer samples were
445 obtained from consented patients treated with ADT (degarelix; 240 mg SQ) in a neo-
446 adjuvant trial (NCT01696877)[1] and matched control radical prostatectomies were
447 obtained from patients treated at the Johns Hopkins Sidney Kimmel Comprehensive
448 Cancer Center (Baltimore, MD) under IRB-approved clinical protocol J1265. All patients
449 provided written, informed consent.

450

451 *Cell Lines*

452 Myc-Cap, derived from spontaneous prostate cancer in c-Myc transgenic mice [2,3], was a
453 generous gift from Dr. C. Sawyers. To generate MCRedAL, Myc-Cap cells were
454 transfected with pRetroQ-mCherry-C1 (Clontech) using lipofectamine 2000 (Invitrogen)
455 and isolated by FACS sorting based on mCherry expression (Extended Data Fig. 1a).
456 Myc-Cap and MCRedAL cells were cultured in DMEM as previously described[2]. LNCaP,
457 VCaP, E006AA, CWR22Rv1, DU145, and PC3 cell lines were obtained and cultured as
458 recommended by the ATCC. LAPC4 (a gift from Dr. S. Yegnasubramanian) were
459 maintained in RPMI-1640 (Corning) supplemented with 10% fetal bovine serum (FBS;
460 Gemini Bio-Products). Androgen independent LNCaP-abl cells were a gift from Dr. Z.
461 Culig and cultured as descrived previously[4]. LAPC4-CR and VCaP-CR (a gift from S.
462 Yegnasubramanian) were derived by passaging LAPC4 and VCaP cells through
463 castrated animals and further subculturing in RPMI-1640 supplemented with 10%
464 charcoal stripped serum (CSS; Gemini Bio-Products) supplemented with 1X B-27

465 Neuronal Supplement (Gibco). For experiments when cells were grown in androgen-free
466 conditions, 10% FBS was substituted for 10% CSS in complete media. For
467 migration/chemotaxis assays, prostate cancer cell lines were cultured in complete media
468 containing either 0.5% or 2.5% FBS for human and murine cells, respectively. All cell
469 lines were cultured in 1% penicillin/streptomycin media at 37°C, 5% CO_2.
470

471 *Mouse Strains*

472 Seven-week-old FVB/NJ, J:NU, C57BL/6-Tg(TcraTcrb)1100Mjb/J (OT-I), and B6.SJL-
473 PtprcaPepcb/BoyJ (CD45.1) male mice were purchased from The Jackson Laboratory.
474 A breeding pair of *Hoxb13-rtTA|TetO-H2BGFP* (HOXB13-GFP) mice[5] was received from
475 UMBC and experimental animals were bred in-house. Animals were kept in a specific
476 pathogen-free facility at either Johns Hopkins University School of Medicine or Columbia
477 University Medical Center. All animal experiments were performed in accordance with
478 protocols approved by the Institutional Animal Care and Use Committee (IACUC) at the
479 respective institutions.
480

481 *Tumor Allografts and Xenografts*

482 Eight-week-old male FVB/NJ and J:NU mice were subcutaneously inoculated with either
483 Myc-Cap or MCRedAL (1×10^6 cells/mouse), and LNCaP or PC3 (3×10^6 cells/mouse) in
484 the right flank, respectively. Tumor diameters were measured with electronic calipers
485 every 3 days as indicated and the tumor volume was calculated using the formula:
486 [longest diameter × (shortest diameter)^2]/2. Myc-Cap tumor bearing mice received
487 androgen-deprivation therapy (ADT) 4 weeks after tumor implantation when tumor

488 volume reached ~500mm^3, as indicated in figure legends. ADT was administered via
489 subcutaneous (sc) injection of degarelix acetate (a GnRH receptor antagonist; Ferring
490 Pharmaceuticals Inc.) at a dosage of 0.625 mg/100 µl H_2O/25 g body weight every 30
491 days, unless otherwise indicated. Onset of castration-resistance was defined as the time
492 to tumor size increased by 30% (~650 mm^3) after ADT. Chemical castration by ADT was
493 compared to bilateral orchiectomy as described in Extended Data Fig. 1a.
494
495 *Luminal Epithelial Regression/Regeneration*
496 Eight-week-old male HOXB13-GFP mice carrying the *Hoxb13-rtTA* transgene and a
497 Tetracycline operator–Histone 2B-Green Fluorescent Protein (TetO-H2BGFP), which
498 results on GFP expression being restricted to luminal epithelial Hoxb13$^+$ cells (described
499 previously[5]), were castrated via bilateral orchiectomy. A cycle of prostate
500 regression/regeneration was induced as described previously[6]. Briefly, mice were
501 allowed to regress for six weeks to reach the fully involuted state. Mice were randomized
502 to ADT or ADT + testosterone (T) treatment groups. Testosterone was administered for
503 four weeks for prostate regeneration by subcutaneous pellets; this regimen yields
504 physiological levels of serum testosterone. All mice received 2mg/ml of Doxycycline
505 (Sigma) in the drinking water to induce GFP expression[5] under the control of the luminal
506 epithelial promoter, HoxB13, one week prior euthanizing them for their analysis.
507
508 *Antibody Blockade*
509 Anti-CXCR2 (murine IgG1-D265A, clone: 11C8; a non-FcγR-binding mutant with
510 deficient FcγR-mediated depletion), anti-CSF1R (rat IgG2a, clone: AFS98; with

511 competent FcγR-mediated depletion), and anti-CTLA-4 (murine IgG2a, clone: 12C11;
512 with competent FcγR-mediated depletion)[7] were used. Antibody treatment was
513 administered via intraperitoneal (ip) injection at a dose of 50 mg/kg body weight for 3
514 doses every 4 days for CXCR2, 50 mg/kg body weight every 3 days for the duration of
515 the experiment for CSF1R, and/or10 mg/kg body weight for 3 doses every 3 days for
516 CTLA-4. Mouse IgG1 (clone: 4F7), rat IgG2a (clone: 2A3), and mouse IgG2a (clone:
517 4C6) were used as isotype controls. Anti-CXCR2 and anti-CSF1R treatments started
518 7 days before ADT; while anti-CTLA-4 treatment was started either 3 or 12 days before
519 ADT ($400mm^3$ vs. $200mm^3$, respectively).
520
521 *Flow cytometry*
522 Single-cell suspensions from prostate tumor and tissues were prepared using the mouse
523 tumor dissociation kit according to the manufacturer's recommendations (Miltenyi).
524 Single-cell suspensions of tumor-draining lymph nodes (TDLNs) and spleens were
525 homogenized mechanically with the back of a syringe. Cells were Fc-blocked with
526 purified rat anti-mouse CD16/CD32 (Clone: 2.4 G2, Becton Dickinson BD) for 15 minutes
527 at RT. Dead cells were discriminated using the LIVE/DEAD (L/D) fixable viability dye
528 eFluor 506 or near-IR dead cell stain kit (Thermo Fisher) and samples were stained for
529 extracellular and intracellular markers. The following antibodies were used: CD45 (30F-
530 11), CD45.2 (104), CD24 (M1/69), CD49f (GOH3), Ly6C (HK1.4), Ly6G (1A8), Gr1 (RB6-
531 8C5), CD11b (M1/70), F4/80 (BM8), MHCII (2G9), PD-L1 (10F.9G2), CD4 (RM4-5), CD8
532 (53-6.7), CD44 (IM7), CD62L (MEL-14), CD25 (PC61), Ki67 (16A8), IFN-γ (XMG1.2),
533 TNF-α (MP6-XT22), IL-2 (JES6-5H4), GZβ (GB11), CXCR2 (242216), and IL-23

534 (FC23CPG). For intracellular staining, cells were fixed and permeabilized using BD
535 Perm/Wash (BD Biosciences) at room temperature for 45 minutes. For intracellular
536 cytokine staining, cells were stimulated with PMA (50 ng/ml) and ionomycin (500 ng/ml)
537 for 4 hours in the presence of protein transport inhibitor cocktail (eBiosciences). Gates
538 of cytokines were determined by fluorescence minus one (FMO) controls. Staining was
539 visualized by fluorescence activated cell sorting (FACS) analysis using a BD
540 FACSCelesta™ (BD Biosciences) and analyzed using FlowJo® (Flowjo LLC). Prostate
541 luminal epithelial cells are defined as $CD45^{-}CD11b^{-}F4/80^{-}CD24^{+}CD49f^{int}GFP^{+}$, and
542 prostate epithelial tumor cells are defined as $CD45^{-}CD11b^{-}F4/80^{-}mCherry^{+}$. Tumor
543 associated macrophages (TAMs) are referred to as $CD45^{+}CD11b^{+}F4/80^{+}$, inflammatory
544 TAMs as $CD45^{+}CD11b^{+}F4/80^{+}Ly6C^{+}MHCII^{-}$, immature TAMs as
545 $CD45^{+}CD11b^{+}F4/80^{+}Ly6C^{+}MHCII^{+}$, $MHCII^{hi}$ TAMs as $CD45^{+}CD11b^{+}F4/80^{+}Ly6C^{-}MHCII^{+}$,
546 $MHCII^{low}$ TAMs as $CD45^{+}CD11b^{+}F4/80^{+}Ly6C^{-}MHCII^{-}$. PMN-MDSCs are defined as
547 $CD45^{+}CD11b^{+}Ly6C^{+}Ly6G^{+}$. CD4 T cells as $CD45^{+}CD4^{+}$, regulatory T cells as
548 $CD45^{+}CD4^{+}CD25^{+}$, CD8 T cells as $CD45^{+}CD8^{+}$, polyfunctional CD8 T Cells as
549 $CD45^{+}CD8^{+}IFN\gamma^{+}TNF\alpha^{+}Gz\beta^{+}$, and memory CD8 T cells as $CD45^{+}$ $CD8^{+}CD44^{+}CD62L^{-}$.
550 123Count eBeads counting beads (Thermo Fisher) were used to normalize the numbers
551 of PMN-MDSCs in migration/chemotaxis experiments.
552
553 *Protein Quantification*
554 Tumors collected at different treatment time points were minced, lysed in CelLytic MT
555 (Sigma) containing halt protease and phosphatase inhibitor (Thermo Fisher) in a 1:100
556 ratio, and incubated on ice for 30 minutes with intermittent vortexing. Tumor lysates were

557 assayed for raw protein concentration with Coomassie assay (Bio-Rad). IL-8 and Cxcl15
558 were analyzed by ELISA kits following the manufacturer's instructions (BD Bioscience
559 and R&D Systems, respectively).
560
561 *Immunohistochemical staining (IHC)*
562 Tumor and tissue samples were fixed with either 10% formalin (Fisher Scientific,
563 Pittsburgh, PA) or zinc fixative (BD) for 24 hours before paraffin embedding and
564 sectioning. Sections were stained with hematoxylin and eosin (H&E), and antibodies
565 against mouse Ly6G (1A8; BD Pharmingen) and F4/80 (BM8; eBioscience). Staining
566 was performed by the Molecular Pathology core of the Herbert Irving Comprehensive
567 Cancer Center at Columbia University. All images were acquired on a Leica SCN 400
568 system with high throughput 384 slide autoloader (SL801) and a 40X objective; files were
569 processed with Aperio ImageScope v12.3.1.6002.
570
571 *RNA In Situ Hybridization (RISH) and Immunohistochemistry*
572 Manual fluorescent RISH was performed on formalin-fixed and zinc-fixed paraffin
573 embedded sections using company protocols. Briefly, 5μm sections were cut, baked at
574 60 ℃ for 1 hour, dewaxed, and air-dried before pre-treatments. RISH *Cxcl15* probe, 3-
575 plex positive control probes (*Polr2a*, *Ppib*, *Ubc*) and 3-plex negative control probes (*DapB*
576 of Bacillus subtilis strain) from Advanced Cell Diagnostics (ACD) were used in this study.
577 Detection of specific probe binding sites was performed with RISH Multiplex Fluorescent
578 Reagent Kit v2 Reagent kit from ACD following the manufacturer's instructions. Tyramide

579 CF568 (Biotium) was used to visualize RISH signal.

580 For a more precise identification of cells expressing *Cxcl15*, RISH was coupled to
581 immunohistochemistry of PanCK (Poly; Dako) and CD45 (30-F11; BD Biosciences).
582 Immediately after RISH detection, samples were permeabilized with 0.2% TBS-Tween 20
583 for 10 minutes at RT, and then blocked with 2.5% of normal goat serum (Vector) for 30
584 minutes at RT. Primary antibody for PanCK was diluted 1/400 in renaissance background
585 reducing diluent (Biocare Medical) and incubated overnight at 4 °C. After washing off the
586 primary antibody, the slides were incubated 15 minutes at RT horseradish peroxidase
587 (HRP) secondary antibody (Vector). Tyramide CF640R (Biotium) was used to visualize
588 PanCK staining. In some cases, CD45 staining was also performed. For this, HRP signal
589 was abolished by a 30 minute incubation at RT with PeroxAbolish (Biocare Medical) and
590 then blocked with 2.5% of normal goat serum (Vector) for 30 minutes at RT. Primary
591 antibody for CD45 was diluted 1/50 in renaissance background reducing diluent (Biocare
592 Medical) and incubated 90 minutes at RT. After washing off the primary antibody, the
593 slides were incubated 15 minutes at RT HRP-secondary antibody (Vector). Tyramide
594 CF488A (Biotium) was used to visualize CD45 staining. All images were acquired on a
595 Nikon A1RMP confocal microscope using a 60X objective. Comparisons of ISH-IHC
596 results were performed using ImageJ.

597

598 *Whole Genome Expression Profiling and Analysis*

599 MCRedAL tumor were harvested when their tumor volume reached ~500mm^3 (CS group),
600 and 7 days after chemical castration (ADT). MCRedAL cells were isolated based on their
601 mCherry$^+$ CD45$^-$ F4/80$^-$ CD11b$^-$ expression by flow sorting on a DakoCytomation MoFlo.

602 RNA was extracted using Trizol LS (Invitrogen) and treated with DNAse-I using RNA
603 clean & Concentrator (Zymo Research). The analysis was performed using Affymetrix
604 Mouse Clariom D (MTA 1.0) array according to the manufacturer's instructions. Resulting
605 CEL files were analyzed in Affymetrix Expression Console (v. 1.4) using the SST-RMA
606 method, and all samples passed the quality control. Log2 probe intensities were
607 extracted from CEL (signal intensity) files and normalized using RMA quantile
608 normalization, then further analyzed using Partek Genomics Suite v6.6. Illustrations
609 (volcano plots, heatmaps, and histograms) were generated using TIBCO Spotfire
610 DecisionSite with Functional Genomics. Gene set enrichment analysis (GSEA) of
611 differently expressed genes was performed using the hallmark gene sets Molecular
612 Signature Database (MSigDB).
613
614 *Nanostring*
615 RNA extraction was performed using the Trizol LS reagent (Thermo Fisher) as per
616 manufacturer's instructions. For NanoString analysis, the nCounter mouse PanCancer
617 Immune Profiling panel was employed using the nCounter Analysis System (NanoString,
618 Seattle, WA). Analysis was conducted using nSolver software (NanoString). Heatmap
619 analyses were performed using The R Project for Statistical Computing (https://www.r-
620 project.org/).
621
622 Pairwise Alignment
623 The homology of the murine chemokines Cxcl1, Cxcl2, Cxcl5, Cxcl15, Cxcl12, and Cxcl17
624 to human IL-8 was evaluated using BLASTP 2.9.0+

625 (https://blast.ncbi.nlm.nih.gov/Blast.cgi?PAGE=Proteins)[8]. Proteins were consider
626 homologous if they shared > 30% amino acid identity[9]. Expected values of <0.05 were
627 consider statistically significant. The expected value includes an inherent Bonferroni
628 correction.
629
630 *Chromatin immunoprecipitation assay (ChIP)-Seq*
631 ChIP-Seq data was obtained from
632 https://www.ncbi.nlm.nih.gov/geo/query/acc.cgi?acc=GSE83860 which contains ChIP-
633 Seq data acquired with androgen receptor (AR) and nuclear factor NF-kappa-B p65
634 subunit (p65) specific antibodies on cell lysates from LNCaP cells cultured under the
635 following treatments: DMSO, DHT, and TNFα. For each treatment the dataset contains
636 two ChIP-Seq replicates pulled down using the AR and p65 antibodies[10]. ChIP-Seq data
637 were aligned to the hg38 reference version using the subread package, and then the BAM
638 files were sorted and indexed using SAMtools. Loci with significant differential binding
639 (FDR = 0.05) of pulled-down proteins to DNA were identified using the csaw package for
640 ChIP-Seq analysis, closely following Lun and Smyth's script[7]. ChIP-Seq visualization
641 was performed using the Integrative Genomics Viewer (IGV) from the Broad Institute
642 (http://software.broadinstitute.org/software/igv/).
643
644 *ChIP-qRT-PCR*
645 Chromatin immunoprecipitation was performed as described[11]. In brief, LNCaP cells
646 were washed with serum-free media and then grown in media containing 10% charcoal
647 stripped FBS for 48 hours. Cells were treated with 100nM DHT or vehicle for 8 hours.

648 DNA was cross-linked with 1% formaldehyde in PBS for 10 minutes and crosslinking was
649 quenched by addition of 0.125 M glycine. Fixed cells were then lysed in lysis buffer (1%
650 SDS, 5mM EDTA, 50mM Tris HCl, pH8.1) and sonicated to a fragment size of 200-600
651 bp using a Covaris water bath sonicator (Woburn, MA). Sheared chromatin was then
652 incubated with primary antibodies (AR [06-680, Millipore], H3K4me3 [ab8580, Abcam],
653 phospho-Ser5 RNA polymerase 2 [ab5131, Abcam], RNA polymerase 2 [4H8, Cell
654 Signaling Technologies] or control IgG [Cell Signaling Technologies]) overnight at 4ºC.
655 Complexes were immobilized on Dynabeads (Thermo Fisher) by incubating for 4 hours
656 at 4ºC. Beads were sequentially washed with TSEI (0.1% SDS, 1% Triton X-100, 2mM
657 EDTA, 20mM Tris HCl, pH 8.1, 150mM NaCl), TSEII (0.1% SDS, 1% Triton X-100, 2mM
658 EDTA, 20mM Tris HCl, pH 8.1, 500mM NaCl) and TSEIII (0.25 M LiCl, 1% NP-40, 1%
659 deoxycholate, 1mM EDTA, 10mM Tris HCl, pH 8.1). DNA was eluted with IP Elution buffer
660 (1% SDS, 0.1M $NaHCO_3$, proteinase K) and incubated at 56ºC for 15 minutes. Enriched
661 DNA libraries were analyzed using primers specific to *IL-8* locus: Forward: 5'
662 AGCTGCAGAAATCAGGAAGG 3' and Reverse: 5' TATAAAAAGCCACCGGAGCA 3'
663 using quantitative (q) RT-PCR. Data is shown as relative enrichment normalized to input
664 DNA.
665
666 *Quantitative (q) RT-PCR*
667 Total RNA was extracted using Trizol (Ambion). cDNA was prepared from total RNA
668 preps using the RNA to cDNA EcoDry Premix (Clontech). Real-time assays were
669 conducted using TaqMan real-time probes (Applied Biosystems). ΔΔ CT method was
670 used for relative gene expression. Expression of the target gene was normalized to the

671 reference gene (18S) and the mean expression level of the control group. LCM samples
672 were normalized to 18S, TBP, and GAPDH reference genes.
673
674 *Laser Capture Microscopy (LCM)*
675 Formalin fixed-paraffin embedded radical prostatectomy specimens, from patients
676 enrolled in a neoadjuvant clinical trial (NCT01696877)[1] who received 240 mg (SQ) of
677 degarelix and matched control cases (patients that did not receive any hormone therapy),
678 were sectioned at a thickness of 8 μm and transferred onto PEN membrane glass slides
679 (Leica). Sections were deparaffinized, hydrated and stained with hematoxylin prior to
680 microdissection. Individual cancer cells and cancer cell clusters were microdissected by
681 a trained pathologist using a LMD 7000 laser capture microscope (Leica). RNA was
682 recovered from the microdisseceted material using the RNeasy FFPE kit (Qiagen).
683 Quantitative RT-PCR was performed as described above. For the analysis, a Mann-
684 Whitney U test was performed.
685
686 *IL-8 and Cxcl15 CRISPR/Cas9 Knock Outs*
687 The 20 bp long gRNA, designed using Deskgen online software, for targeting *IL-8* and
688 *Cxcl15* in exon 3 (5'- *TTCAGTGTAAAGCTTTCTGA* -3' and 5'-
689 *ACAGAGCAGTCCCAAAAAAT* -3', respectively) were incorporated into two
690 complementary 100-mer oligonucleotides and cloned into a gRNA containing plasmid
691 containing the (NeoR/KanR) cassette (Addgene # 41824). The human codon optimized
692 pCAGGS-Cas9-mCherry was used for gene-editing experiments (a gift from Stem Cell
693 Core Facility at Columbia University). gRNA and Cas9 containing plasmids were

694 introduced to prostate epithelial cells using the basic nucleofector kit (Amaxa, Lonza)
695 following the manufacturer's instructions for primary mammalian epithelial cells (program
696 W001). Successfully transfected cells were selected by culturing in the presence of
697 400µg/ml of neomycin sulfate analog (G418; Sigma), and isolated based on their mCherry
698 expression 24 hours after transfection. Knock out clones were screened for IL-8 and
699 Cxcl15 expression by ELISA and gene-editing confirmed by PCR amplification and
700 Sanger sequencing (GENEWIZ) using primers ~200bp away from the cut site (IL-8
701 Forward: 5'- TTTGGACTTAGACTTTATGCCTGAC -3; IL-8 Reverse: 5'-
702 TCCTGGGCAAACTATGTATGG -3; Cxcl15 Forward: 5'-
703 GCTAGGCACACTGATATGTGTTAAA -3; Cxcl15 Reverse: 5'-
704 ACATTTGGGGATGCTACTGG -3).
705
706 *Migration/Chemotaxis Assay*
707 Cells and supernatants used in this assay were resuspended in culture media containing
708 0.5% or 2.5% FBS. Transwell plates of 3-mm pore size were coated with Fibronectin
709 (Corning Costar) and loaded with 500 ml of medium or with different cell supernatants in
710 triplicates (lower chamber). Cells were resuspended at $2x10^7$ cells/ml, and 200 ml of this
711 suspension was placed in each of the inserts (upper chamber). After 2.5 hours of
712 incubation at 37°C and 5% CO_2, inserts were removed and 10,000 beads (Thermo Fisher)
713 were added to each well. In some cases, either isotype or anti-CXCR2 (200 µg/ml) were
714 added at the beginning of the experiment. The cells in the lower chamber were collected
715 along with the starting cell population, stained with L/D, CD11b, Ly6C, and Ly6G and
716 evaluated by flow cytometry in a BD FACSCelesta™ (BD Biosciences). The ratio of beads

717 to cells was determined, allowing calculation of the number of cells that had migrated to
718 the bottom well. *In vivo*, LD-PMN-MDSCs were collected as described below from
719 splenocytes of CR-Myc-Cap tumor bearing mice and labeled with DiD (DiIC18(5) or 1,1'-
720 Dioctadecyl-3,3,3',3'-
721 Tetramethylindodicarbocyanine, 4-Chlorobenzenesulfonate Salt; Invitrogen), a lipophilic
722 membrane dye, as described previously[12]. DiD^+ LD-PMN-MDSCs were adoptively
723 transferred into FVB/NJ recipient 8-week male mice and their ability to migrate in
724 response to 200ng of recombinant Cxcl15 was evaluated 4 hours after injection. Beads
725 were also used to calculate absolute numbers of $Ly6G^+$ PMNs and DiD^+ LD-PMN-MDSCs
726 *in vivo*.
727
728 *PMN-MDSC Enrichment*
729 Animals were sacrificed and spleens were collected. After dissociating cell clumps, the
730 cell suspension was centrifuged (740 g, 10 minutes, RT) and resuspended in 1 ml HBSS–
731 EDTA containing 0.5% BSA. Cells were then resuspended in 50% Percoll solution and
732 treated on a three-layer Percoll gradient (55%, 72%, and 81%) at (1500 g, 30 minutes,
733 10°C without break). LD-PMN-MDSCs were collected from the 50-55% and 55-72%
734 interfaces. Red blood cells (RBCs) were eliminated with RBC lysis solution (Miltenyi).
735
736 *In vitro Suppression Assays*
737 PMN-MDSCs were isolated from the spleen of CR-Myc-Cap-tumor bearing mice using
738 the neutrophil isolation kit (Miltenyi) according to the manufacturer's instructions; greater
739 than 95% enrichment was confirmed by flow cytometry. Unless otherwise indicated, a

740 density gradient separation was performed prior to column purification. OT-I (CD45.2)
741 transgenic splenocytes were mixed at a 1:10 ratio with sex-matched CD45.1 splenocytes.
742 Splenocytes containing CD8 T responder cells were stained with CellTrace Violet (5μM
743 CTV; Thermo Fisher) and plated on a 96-well round-bottom plate at a density of $2x10^5$
744 cells per well. PMN-MDSCs cells were added at 2-fold dilutions starting from $2x10^5$ cells,
745 in the presence of their cognate peptides (5pM OVA) and incubated for 60 hours.
746 Proliferation of CD8 T responder cells (gated as $L/D^-CD8^+CTV^+$) was quantified by flow
747 cytometry based on the dilution of Cell Trace Violet (CTV). Percent suppression (%
748 Suppression) was calculated by the following formula: % Suppression = [1-(% divided
749 cells of the condition/ the average of % divided cells of T responder only conditions)] x
750 100.
751
752 *Z-score Analysis*
753 IL-8 expression was evaluated in a publicly available data set (GSE8466)[13] using z-score
754 values of quantile-normalized microarray transcripts from benign prostate biopsies. Z-
755 score values were obtained by scaling the data for each gene in each patient to:
756 (expression - mean expression across all genes) / (standard deviation of expression
757 across all genes).
758
759 *Statistical Analysis*
760 Statistical analysis was performed using Prism 7 (GraphPad). Unpaired two-tailed t-tests,
761 Mann-Whitney U test, Tukey's multiple comparisons tests, or Wilcoxon rank sum tests
762 were conducted and considered statistically significant at *p*-values ≤0.05 (*), 0.01 (**),

763 0.001 (***) and 0.0001 (****).

764

765 **Methods References**

766 1 Antonarakis, E. S. *et al.* Neoadjuvant randomized trial of degarelix (Deg) ±
767 cyclophosphamide/GVAX (Cy/GVAX) in men with high-risk prostate cancer (PCa)
768 undergoing radical prostatectomy (RP). *Journal of Clinical Oncology* **35**, 5077-
769 5077, doi:10.1200/JCO.2017.35.15_suppl.5077 (2017).

770 2 Watson, P. A. *et al.* Context-dependent hormone-refractory progression revealed
771 through characterization of a novel murine prostate cancer cell line. *Cancer Res*
772 **65**, 11565-11571, doi:10.1158/0008-5472.CAN-05-3441 (2005).

773 3 Ellwood-Yen, K. *et al.* Myc-driven murine prostate cancer shares molecular
774 features with human prostate tumors. *Cancer cell* **4**, 223-238 (2003).

775 4 Culig, Z. *et al.* Switch from antagonist to agonist of the androgen receptor
776 bicalutamide is associated with prostate tumour progression in a new model
777 system. *Br J Cancer* **81**, 242-251, doi:10.1038/sj.bjc.6690684 (1999).

778 5 Rao, V. *et al.* A Hoxb13-driven reverse tetracycline transactivator system for
779 conditional gene expression in the prostate. *Prostate* **72**, 1045-1051,
780 doi:10.1002/pros.22490 (2012).

781 6 Wang, X. *et al.* A luminal epithelial stem cell that is a cell of origin for prostate
782 cancer. *Nature* **461**, 495-500, doi:10.1038/nature08361 (2009).

783 7 Shen, Y. C. *et al.* Combining intratumoral Treg depletion with androgen deprivation
784 therapy (ADT): preclinical activity in the Myc-CaP model. *Prostate Cancer Prostatic*
785 *Dis* **21**, 113-125, doi:10.1038/s41391-017-0013-x (2018).

786 8 Altschul, S. F. *et al.* Protein database searches using compositionally adjusted
787 substitution matrices. *Febs J* **272**, 5101-5109, doi:10.1111/j.1742-
788 4658.2005.04945.x (2005).
789 9 Pevsner, J. *Bioinformatics and functional genomics*. (John Wiley & Sons, 2015).
790 10 Malinen, M., Niskanen, E. A., Kaikkonen, M. U. & Palvimo, J. J. Crosstalk between
791 androgen and pro-inflammatory signaling remodels androgen receptor and NF-
792 kappaB cistrome to reprogram the prostate cancer cell transcriptome. *Nucleic*
793 *Acids Res* **45**, 619-630, doi:10.1093/nar/gkw855 (2017).
794 11 Haffner, M. C. *et al.* Androgen-induced TOP2B-mediated double-strand breaks
795 and prostate cancer gene rearrangements. *Nat Genet* **42**, 668-675,
796 doi:10.1038/ng.613 (2010).
797 12 Carlson, A. L. *et al.* Tracking Single Cells in Live Animals Using a Photoconvertible
798 Near-Infrared Cell Membrane Label. *Plos One* **8**, doi:ARTN e69257
799 10.1371/journal.pone.0069257 (2013).
800 13 Mostaghel, E. A. *et al.* Intraprostatic androgens and androgen-regulated gene
801 expression persist after testosterone suppression: therapeutic implications for
802 castration-resistant prostate cancer. *Cancer Res* **67**, 5033-5041,
803 doi:10.1158/0008-5472.CAN-06-3332 (2007).